Supplement of Hydrol. Earth Syst. Sci., 30, 3221–3244, 2026
https://doi.org/10.5194/hess-30-3221-2026-supplement

Hydrology and Earth System Sciences
Open Access
EGU

Supplement of

Reconstruction of climate-driven global terrestrial water storage variations (2002–2021) using a four-parameter linear recursive model

Pu Xie and Shuang Yi

Correspondence to: Shuang Yi (s.yi@ucas.ac.cn)

Table S1. The Nash–Sutcliffe efficiency results between the reconstructed values and GRACE JPLM, calibrated according to Eq. (8) based on ERA5-Land precipitation and temperature. River basin IDs are sorted in descending order of their corresponding area (unit:$10^4\ km^2$).

ID	Basins	NSE	Area	ID	Basins	NSE	Area
1	Amazon	0.85	596.59	59	Uruguay	0.90	26.61
2	Congo	0.61	370.52	60	Magdalena	0.82	26.07
3	Nile	0.82	335.32	61	Krishna	0.87	25.88
4	Mississippi	0.89	324.06	62	Haihe	0.65	25.02
5	Ob	0.91	304.06	63	Thelon	0.68	24.49
6	Parana	0.82	264.70	64	Yana	0.64	23.34
7	Yenisei	0.73	250.57	65	Fraser	0.71	23.08
8	Chad	0.74	247.10	66	Har Us Nuur	0.76	22.90
9	Lena	0.64	245.36	67	Liao He	0.73	22.01
10	Amur	0.87	223.90	68	Olenek	0.56	21.77
11	Niger	0.37	212.30	69	Ogooue	0.67	21.52
12	Mackenzie	0.76	179.56	70	Ural	0.67	21.10
13	Yangtze	0.75	174.81	71	Kura	0.74	18.98
14	Tarim He	0.49	156.32	72	Lake Turkana	0.74	18.12
15	Volga	0.87	142.44	73	Rufiji	0.87	17.71
16	Zambezi	0.96	137.81	74	Cuvelai	0.87	17.42
17	Aral Sea	0.77	137.25	75	Anadyr	0.72	17.21
18	Lake Eyre	0.89	121.46	76	HuaiHe	0.67	17.21
19	Nelson	0.90	110.65	77	Pyasina	0.75	16.96
20	Murray	0.87	105.54	78	Ruvuma	0.79	16.41
21	Saint Lawrence	0.79	105.33	79	Rhine	0.75	16.31
22	Ganges	0.84	100.66	80	Chao Phraya	0.66	15.77
23	Orange	0.88	97.73	81	Sacramento and San Joaquin river basin	0.90	15.49
24	Yellow River	0.81	96.30	82	Chuy (Shu)	0.58	15.30

25	Orinoco	0.75	94.14	83	Taz	0.69	15.03
26	Shatt Al Arab	0.92	93.56	84	Cuanza	0.60	15.01
27	Indus	0.81	86.50	85	Red	0.75	14.80
28	Yukon	0.61	83.28	86	Melrhir	0.81	14.64
29	Jubba	0.78	79.79	87	Elbe	0.80	13.84
30	Danube	0.88	79.53	88	Chobut	0.30	13.79
31	Mekong	0.74	78.38	89	Chubut	0.33	13.79
32	Tocantins	0.81	77.25	90	Great Salt Lake	0.82	13.63
33	Okavango	0.88	69.22	91	Negro	0.76	13.61
34	Rio Grande	0.77	67.39	92	Caniapiscau	0.50	13.55
35	Columbia	0.83	66.94	93	Mahanadi	0.68	13.55
36	Colorado	0.81	66.11	94	Albany	0.53	13.47
37	Kolyma	0.73	65.30	95	Santiago	0.72	13.41
38	Sao-Francisco	0.87	63.72	96	Sarysu	0.70	13.41
39	Brahmaputra	0.43	54.08	97	Sanaga	0.37	13.36
40	Dnieper	0.88	50.98	98	Burdekin	0.86	13.04
41	Senegal	0.72	45.80	99	Mar Chiquita	0.88	12.99
42	Don	0.92	43.77	100	Usumacinta	0.89	12.74
43	Rio De La Plata	0.90	42.73	101	Kuskokwim	0.60	12.31
44	Irrawaddy	0.58	42.29	102	ABHE BAD	0.49	12.00
45	Lake Balkhash	0.72	41.48	103	Guir	0.75	12.00
46	Limpopo	0.86	41.26	104	Hamun-I-Mashkel	0.92	11.89
47	Volta	0.76	41.26	105	Oder	0.82	11.88
48	Zhujiang	0.66	40.63	106	Brazos	0.90	11.86
49	Hamun	0.76	40.06	107	Loire	0.72	11.67
50	Indigirka	0.57	34.12	108	Rharsa	0.83	11.44
51	Parnaiba	0.87	33.30	109	Lake Gairdner	0.79	11.31
52	Pechora	0.73	31.42	110	Mobile River	0.83	11.25
53	Godavari	0.72	31.04	111	Pur	0.70	11.13

54	N.Dvina	0.75	30.68	112	Kunene	0.88	10.89
55	Severnaya Dvina	0.75	30.68	113	Flinders	0.76	10.78
56	Khatanga	0.55	30.08	114	Moose	0.77	10.77
57	Neva	0.87	28.15	115	Save	0.81	10.26
58	Salween	0.70	26.63	116	Victoria	0.82	10.11

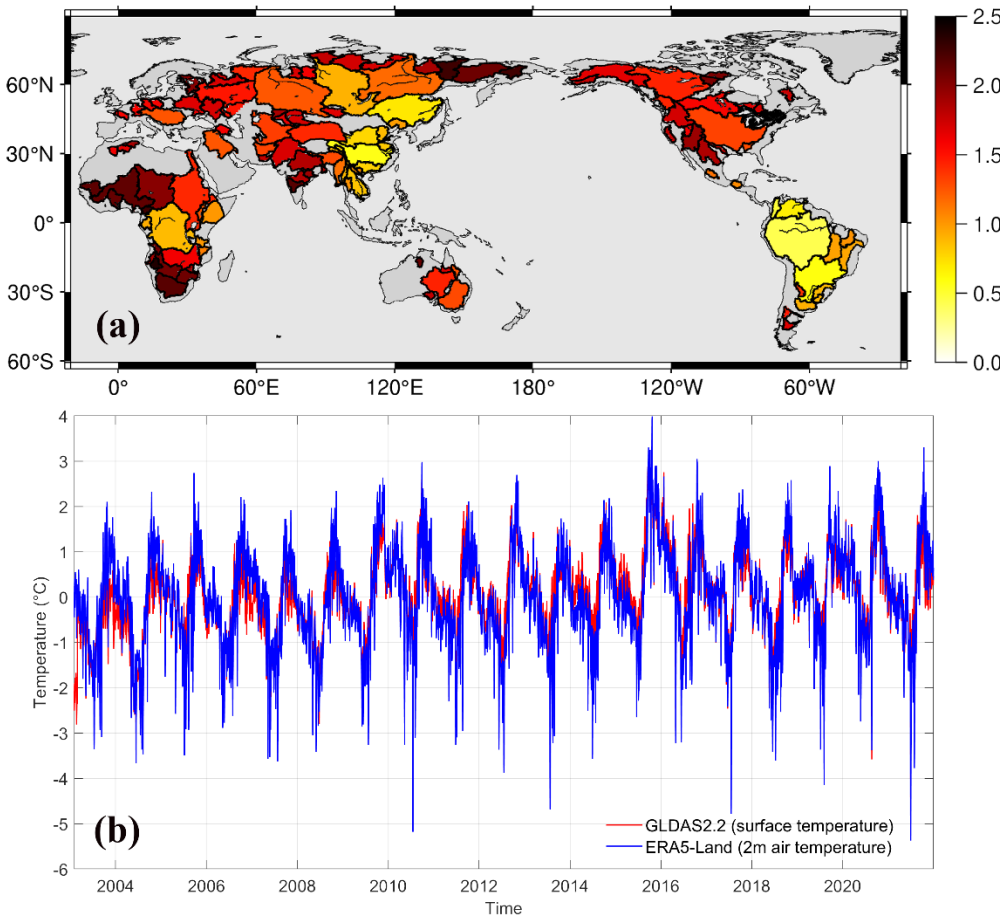

Figure S1. Spatial distribution of RMS differences between ERA5-Land 2 m air temperature and GLDAS-2.2 surface temperature over 116 global river basins (a). Comparison of daily ERA5-Land 2 m air temperature and GLDAS-2.2 surface temperature over the Amazon basin (b).

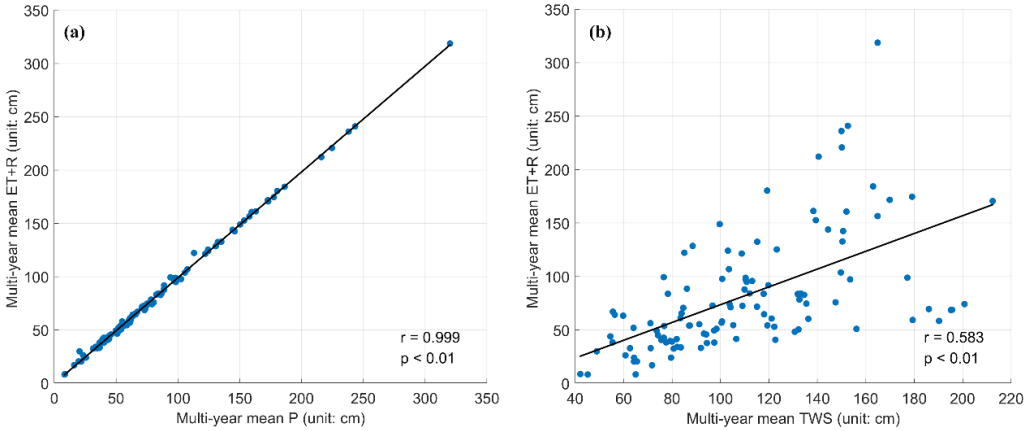

Figure S2. Scatter plot of multi-year mean precipitation versus multi-year mean evapotranspiration plus runoff $(ET + R)$ for each basin (a). Scatter plot of multi-year mean TWS versus multi-year mean $ET + R$ for each basin (b). The black dashed line denotes the linear regression fit. Pearson correlation coefficient r and the p-value for the regression slope are annotated on each panel.

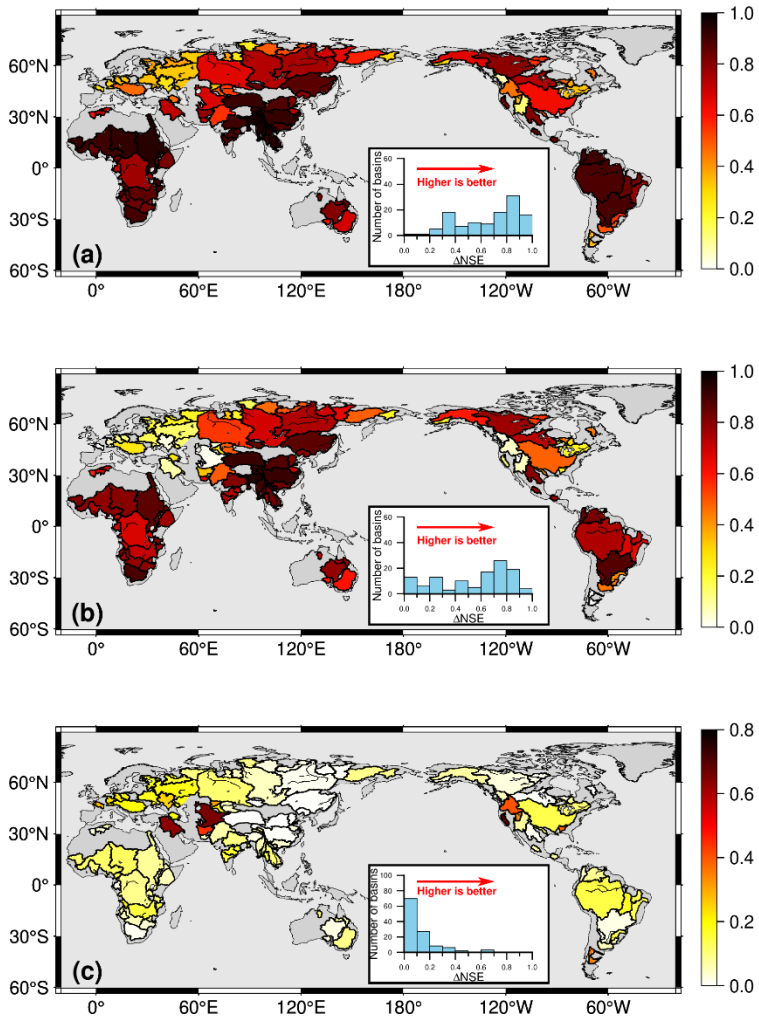

Figure S3. (a) Spatial distribution of the coefficient of determination (R^2) from the multiple linear regression model $ETR = x \cdot P(t) + y \cdot TWS(t-1)$; (b) Spatial distribution of R^2 from the univariate linear regression $ETR = x \cdot P(t)$; (c) Map of the difference between panels (a) and (b) .All basins pass the F-test at the 1% significance level ($p < 0.01$).

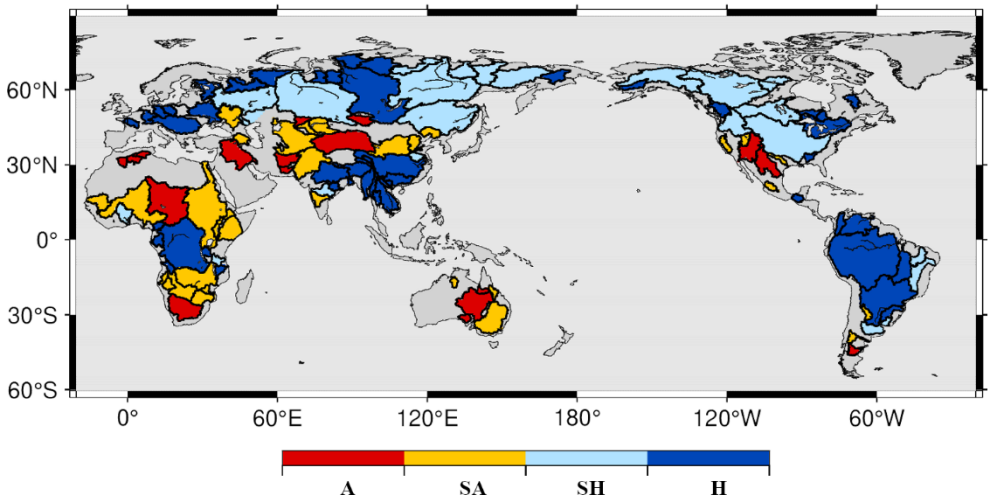

Figure S4. Spatial distribution of the 116 study river basins classified by mean-annual aridity index (AI). Colors denote four climate classes—humid (H), sub-humid (SH), semiarid (SA) and arid (A).

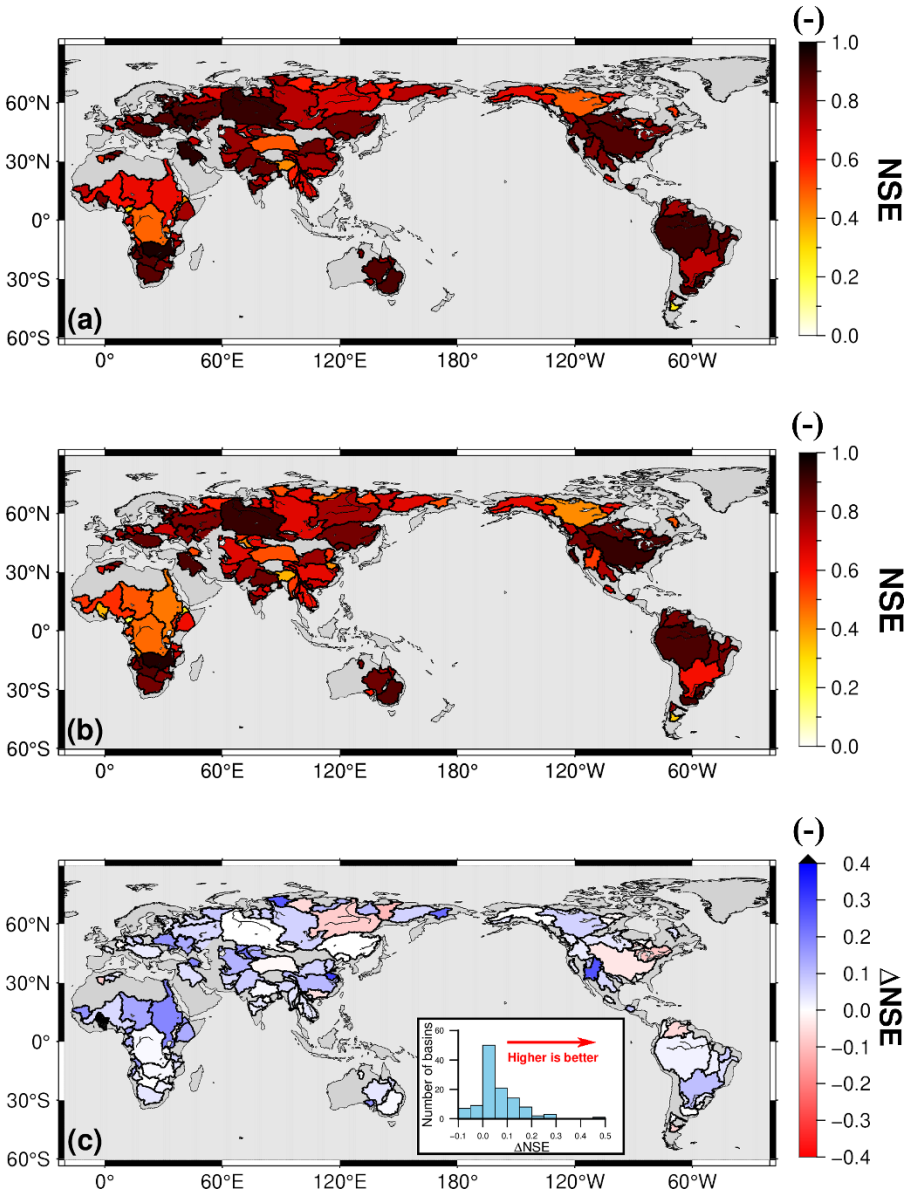

Figure S5. Spatial distribution of NSE (de-seasonalized, de-trended anomalies) between JPLM and two reconstruction models across 116 global river basins during 2002–2019. The NSE between JPLM and JPL-REC (a); the NSE between JPLM and Humphrey-JPL-REC (b); and their difference (ΔNSE=JPL-REC - Humphrey-JPL-REC) (c). The inset histogram in (c) illustrates the distribution of ΔNSE across all basins, where positive values indicate better agreement with GRACE observations by our reconstruction model.

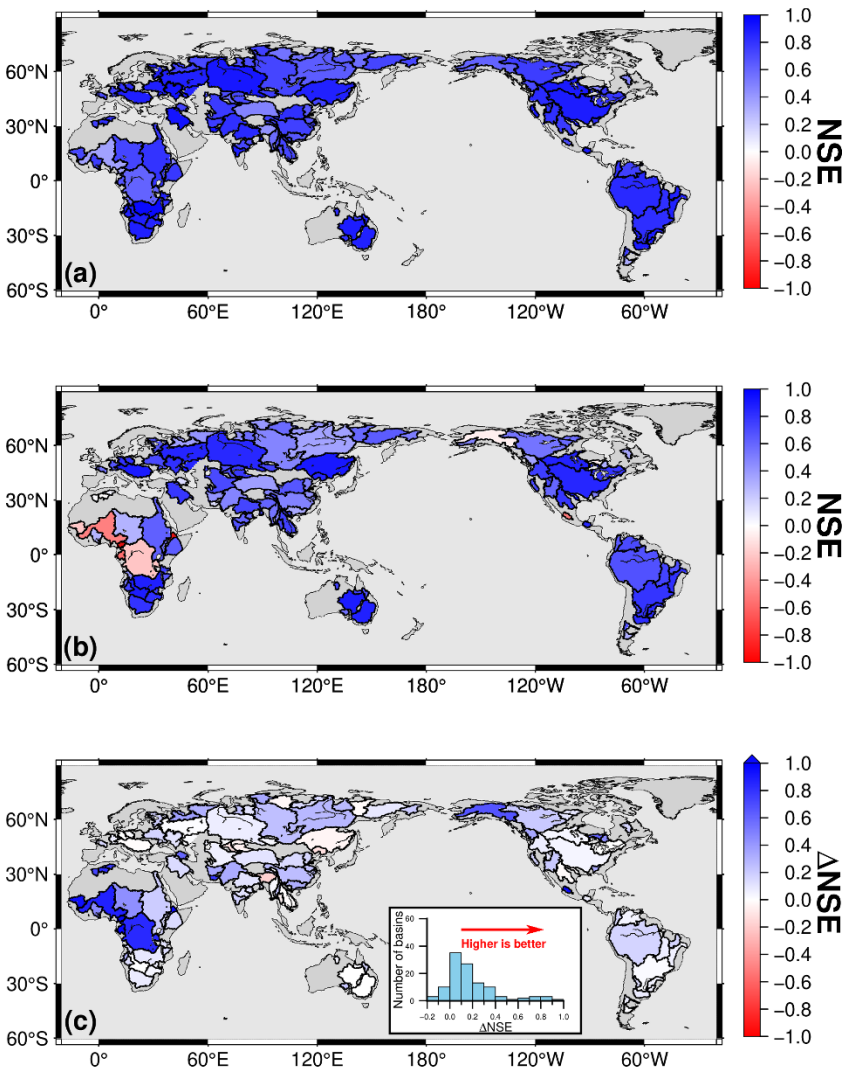

Figure S6: Spatial distribution of the NSE of de-seasonalized, de-trended TWSA between JPLM and (a) JPL-REC and (b) GLDAS GLMS across 116 global river basins for 2003–2021; (c) their difference ($\Delta NSE = (a) - (b)$). The inset histogram in (c) illustrates the distribution of ΔNSE across all basins, where positive values indicate better agreement with GRACE observations by our reconstruction model.

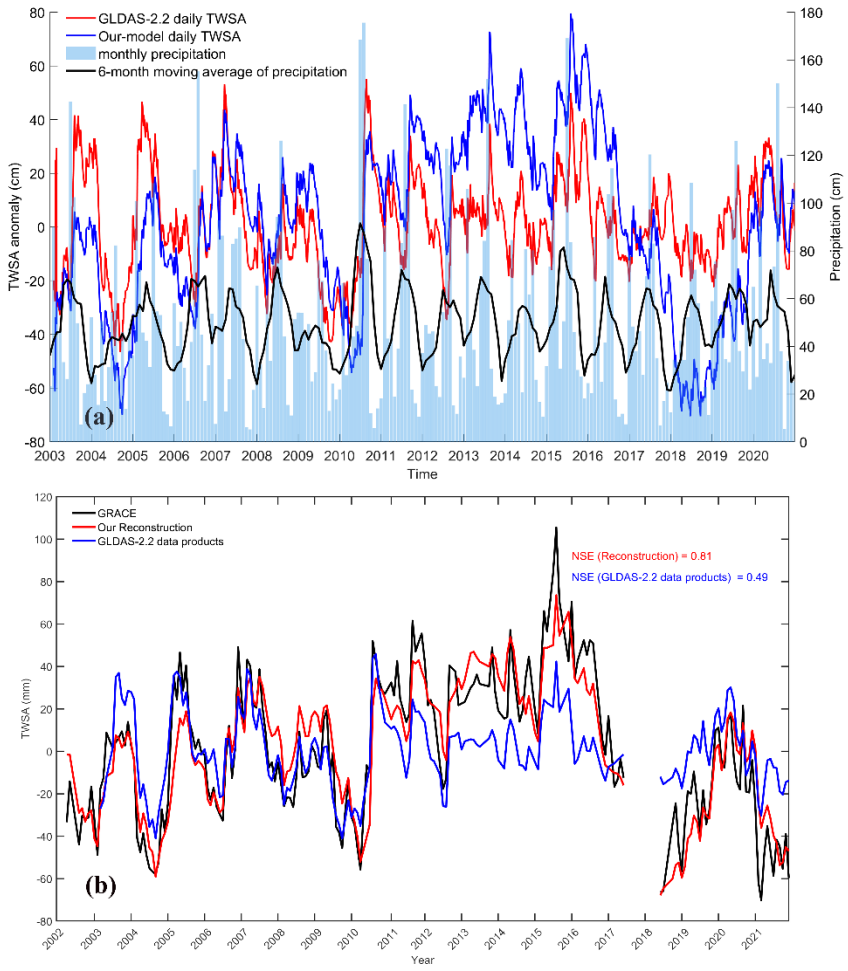

Figure S7: Comparison of daily and monthly TWSA reconstruction in the Indus River basin. (a) Detrended and deseasonalized daily TWSA from GLDAS-2.2(red line), our model-based daily TWSA reconstruction (blue line), monthly precipitation (light blue bars), and 6-month moving average precipitation (black line); (b) Monthly GRACE TWSA, model-based monthly TWSA reconstruction, and monthly TWSA aggregated from daily GLDAS-2.2 data.

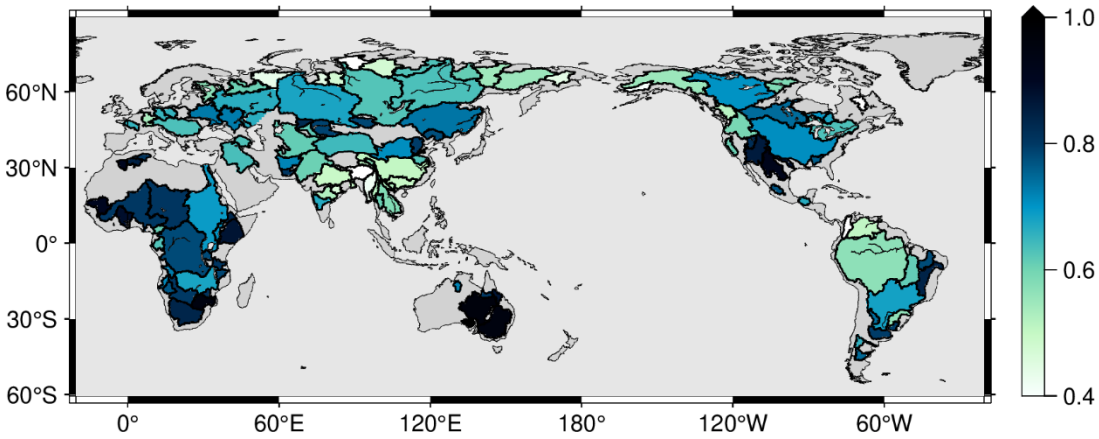

Figure S8. Spatial distribution of the proportion of multi-year mean evapotranspiration (ET) relative to multi-year mean precipitation (P).

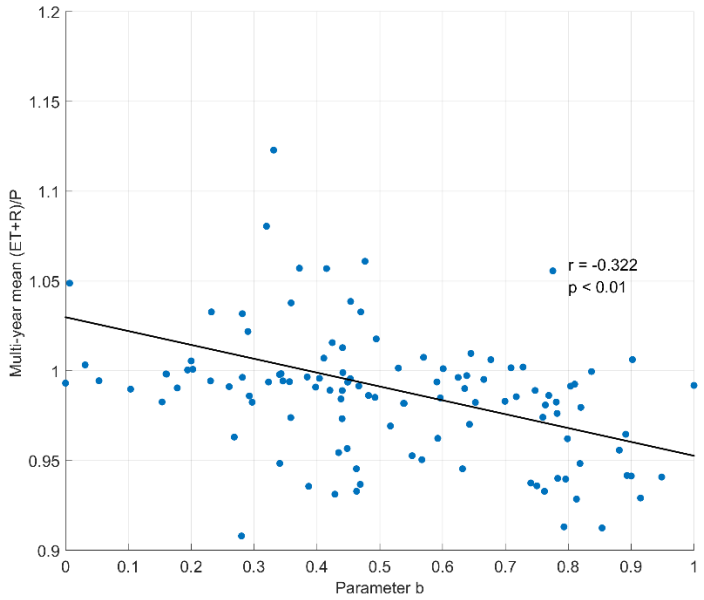

Figure S9. Scatter relationships across 116 global river basins between parameter b and the long-term mean loss ratio $(ET + R)/P$. The black dashed line denotes the linear regression fit. Pearson correlation coefficient r and the p-value for the regression slope are annotated on each panel.

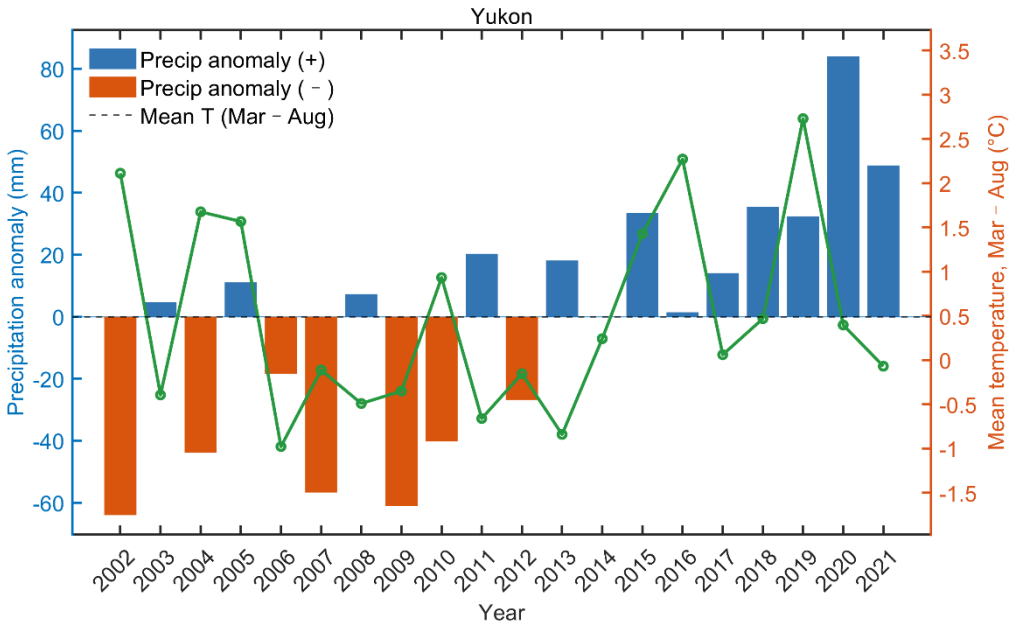

Figure S10. Annual precipitation and mean temperature during the snowmelt season (March–August) in the Yukon River Basin

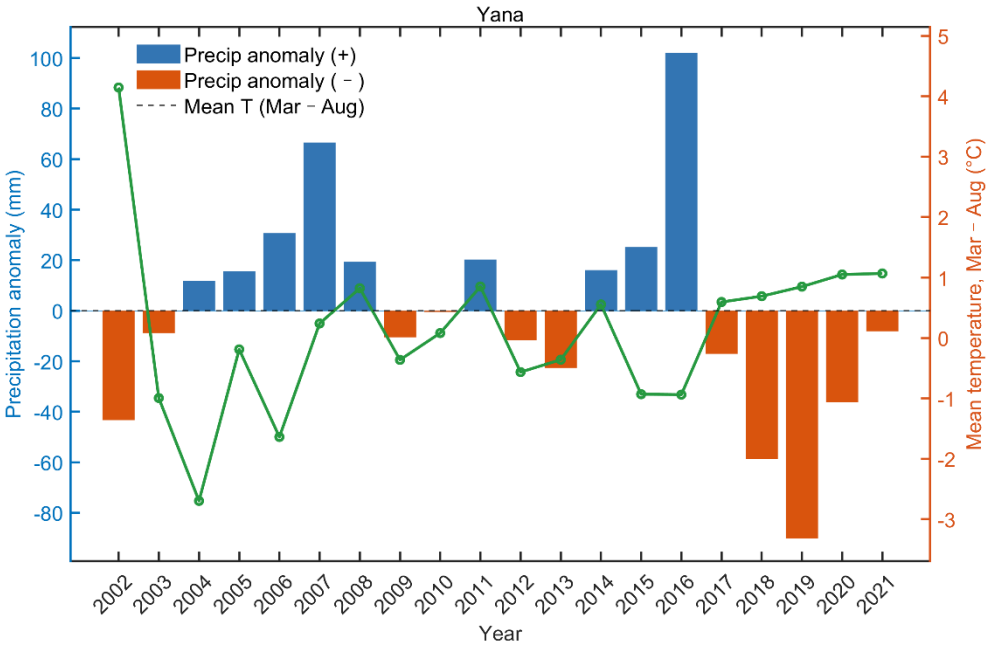

Figure S11. Annual precipitation and mean temperature during the snowmelt season (March–August) in the Yana River Basin